Journal of Power Sources 247 (2014) 545–550

Contents lists available at ScienceDirect

Journal of Power Sources

journal homepage: www.elsevier.com/locate/jpowsour

Short communication

Facile synthesis of large-area CeO_2/ZnO nanotube arrays for enhanced photocatalytic hydrogen evolution

Cheng-hui Zeng [a, b], Shilei Xie [a], Minghao Yu [a], Yangyi Yang [a], Xihong Lu [a, *], Yexiang Tong [a, *]

[a] KLGHEI of Environment and Energy Chemistry, MOE of the Key Laboratory of Bioinorganic and Synthetic Chemistry, School of Chemistry and Chemical Engineering, Sun Yat-Sen University, Guangzhou 510275, China
[b] College of Chemistry and Chemical Engineering, Jangxi Normal University, Nanchang 330022, China

HIGHLIGHTS

- Design of CeO_2/ZnO nanotube array films via a simple two-step electrodeposition process.
- CeO_2/ZnO nanotube arrays exhibit enhanced photocatalytic activity and excellent stability.
- Films on FTO substrates make the collection and recycle of photocatalyst easier.

GRAPHICAL ABSTRACT

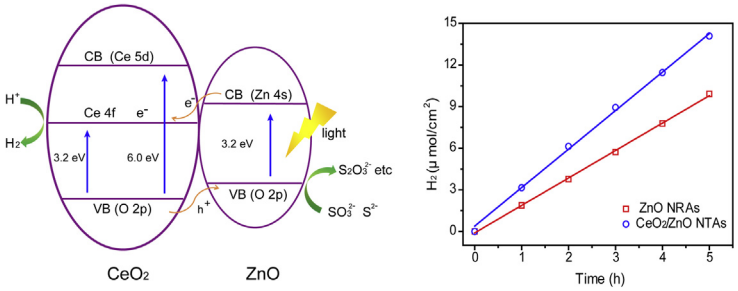

ARTICLE INFO

Article history:
Received 20 July 2013
Received in revised form
2 September 2013
Accepted 3 September 2013
Available online 12 September 2013

Keywords:
Ceria
Zinc oxide
Nanotube
Hydrogen evolution

ABSTRACT

CeO_2/ZnO nanotube array films grown on FTO substrates are successfully synthesized by a two-step electrodeposition process. The CeO_2/ZnO nanotube array films exhibit substantially enhanced photocatalytic activity with a hydrogen evolution rate of 2.7 μmol cm^{-2} h^{-1} under white light irradiation and excellent stability. Moreover, the collection and recycle of these immobilized CeO_2/ZnO nanotube array films are much easier compared with the powder photocatalysts.

1. Introduction

As a clean energy carrier without greenhouse gases or other pollutants, hydrogen has gained great interest owing to the increasing demand for energy and environment protection. Searching an effective and low-cost approach to produce hydrogen is very important for hydrogen economy. Photocatalytic hydrogen production is widely recognized as one of the most promising approaches to generate hydrogen, which is produced in a sustainable manner from solar energy without yielding carbon dioxide [1,2]. Recently, nanostructures have received considerable interest for photocatalytic hydrogen production due to their high surface area and rapid charge separation ability. Among various nanostructures, hollow nanotubes are attracting a great deal of attention as photocatalysts because they have higher interfacial area and faster charge transport pathway than nanoparticles and other one-

* Corresponding authors. Tel.: +86 20 84110071; fax: +86 20 84112245.
E-mail addresses: luxh6@mail.sysu.edu.cn, luxihong@gmail.com (X. Lu).

0378-7753/$ – see front matter © 2013 Elsevier B.V. All rights reserved.
http://dx.doi.org/10.1016/j.jpowsour.2013.09.015

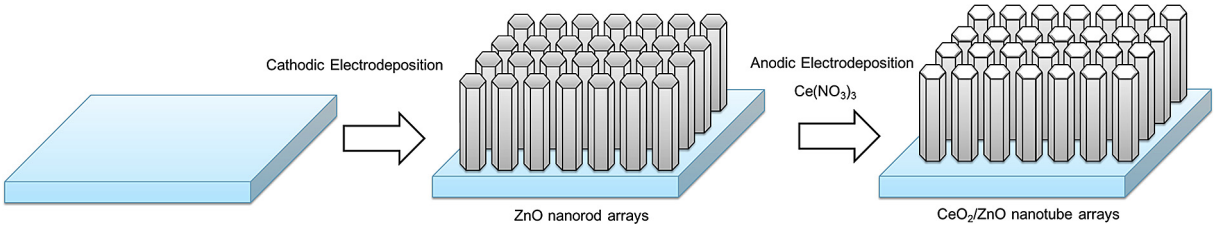

Fig. 1. Schematic diagram of the fabrication process for CeO_2/ZnO nanotube arrays.

dimensional (1D) nanostructures such as nanorods or nanowires [3,4]. Moreover, recent reports have demonstrated that the direct growth of ordered nanotubes on conductive substrates can facilitate the diffusion of active species and transport of electrons, and could further improve photocatalytic performance [5,6]. In recent years, numerous methods including high temperature evaporation, hydrothermal synthesis, anodic oxidation, and template- and surfactant-assisted growth techniques have been developed to prepare nanotubes on conductive substrates [7–11]. Nevertheless, the development of facile, low-cost and effective methods for the large-area synthesis of ordered nanotubes on conductive substrates is highly desirable, but still challenging.

Transition metal oxides such as TiO_2, ZnO and $BiVO_4$ have been extensively investigated as photocatalysts for photocatalytic hydrogen production [12–17]. Little attention has been paid to the rare earth oxides, regardless of their outstanding optical and catalytic properties. In recent years, CeO_2 has attracted increasing interest as a photoactive material because it has strong redox capability, and a relatively small band gap of 3.2 eV that originates from the O 2p to Ce 4f transition [18]. Additionally, CeO_2 nanostructures such as hexagonal nanorods and nanowires have been examined in photocatalytic hydrogen evolution, and they have shown good photocatalytic activity [6,19,20]. However, the large-scale fabrication of CeO_2 nanostructures with good photocatalytic activity, especially for commercial manufacture, is still very challenging. In this paper, we report a facile and cost-effective electrochemical method to synthesize large-area CeO_2/ZnO nanotube arrays (NTAs) on F-doped SnO_2 (FTO) glass substrates and their improved performance in photocatalytic hydrogen production. The CeO_2/ZnO nanotube arrays were grown on FTO substrates via a two-step electrodeposition process, which involves the cathodic electrodeposition of aligned ZnO nanorod arrays (NRAs) as the template and subsequently anodic electrodeposition of CeO_2 on the ZnO nanorods to form CeO_2/ZnO nanotubes. These CeO_2/ZnO nanotube arrays grown directly on FTO substrates can provide a high interfacial area and superior electron transport pathways, which hence improve their photocatalytic performance. The CeO_2/ZnO nanotube arrays exhibited substantially higher photocatalytic activity than ZnO nanorod arrays, with a hydrogen evolution rate of 2.7 μmol cm^{-2} h^{-1} under white light irradiation and good cycling performance.

2. Experimental

2.1. Materials

The analytical grade of commercially $Zn(NO_3)_2$ (Sinopharm Chemical Reagent Co., Ltd., Beijing, China), $Ce(NO_3)_3$ (Sinopharm Chemical Reagent Co., Ltd., Beijing, China), ammonium acetate (NH_4Ac) (Sinopharm Chemical Reagent Co., Ltd., Beijing, China), hexamethylenetetramine (HMT) (Sinopharm Chemical Reagent Co., Ltd., Beijing, China) and dimethyl sulfoxide (Sinopharm Chemical Reagent Co., Ltd., Beijing, China) were used directly without any purification. The F-doped SnO_2-coated glass (FTO, TCO-15) with a sheet resistance of 14 <OMEGA> per square was purchased from Nippon Sheet Glass Co., Ltd., Tokyo, Japan. The FTO glass was cleaned ultrasonically in distilled water, ethanol, and acetone and then rinsed in distilled water again before electrodeposition.

2.2. Photocatalysts preparation

The CeO_2/ZnO nanotube arrays were synthesized by a two-step electrodeposition process, which is summarized schematically in Fig. 1. First, ZnO nanorod arrays were grown on FTO substrates (4 × 4 cm^2) by cathodic electrodeposition in an aqueous solution containing 0.02 M $Zn(NO_3)_2$, 0.01 M NH_4Ac and 0.01 M HMT with a current density of 0.5 mA cm^{-2} at 90 °C. After 60 min cathodic deposition, a white film was obtained on FTO substrate. The ZnO nanorod arrays were then used as templates for further formation of CeO_2/ZnO nanotube arrays. CeO_2/ZnO nanotubes were directly obtained via anodic electrodeposition in a solution of 0.01 M $Ce(NO_3)_3$ + 10% DMSO (10 vol % DMSO:90 vol % H_2O) with a current density of 0.25 mA cm^{-2} at 90 °C.

2.3. Characterizations and measurements

The surface morphologies and microstructures were analyzed by a field-emission scanning electron microscope (FE-SEM, JSM-6330F) and transmission electron microscopy (TEM, JEM-2010F). The structures of the samples were investigated via an X-ray diffractometer (XRD, D8 ADVANCE) using Cu Kα radiation (λ = 0.15418 nm). The chemical state of the films was analyzed directly using X-ray photoelectron spectroscopy (XPS, ESCA-Lab250). The optical properties of the products were measured with a UV–Vis–NIR Spectrophotometer (UV–Vis–NIR, Shimadzu UV-2450).

The photocatalytic hydrogen evolution reactions were examined in a closed gas circulation and evacuation system. Typically, a piece of large-area ZnO or CeO_2/ZnO films (4 × 4 cm^2) was immersed into 100 mL of 0.1 M Na_2S and 0.1 M Na_2SO_3 mixed aqueous solution in a Pyrex reaction cell. The light source was a 300 W Xe lamp (PLS-SXE-300UV, Beijing Trusttech) supplying the full wavelength illumination. The intensity of the white light was determined by an irradiatometer (BNU photoelectric Co., Ltd., FZ-A) and was about 100 mW cm^{-2}. The amount of hydrogen produced was analyzed using on-line gas chromatography (with a thermal conductivity detector and an N_2 carrier).

3. Results and discussion

Fig. 2a is the photo image of CeO_2/ZnO nanotube arrays obtained on FTO substrate, showing that most of the FTO substrate (around 16 cm^2) was uniformly covered by a thin film with good transmittance. Scanning electron microscopy (SEM) images in Fig. 2b and c clearly show that the white film obtained on FTO substrate was covered by dense and ordered ZnO nanorods. These nanorods

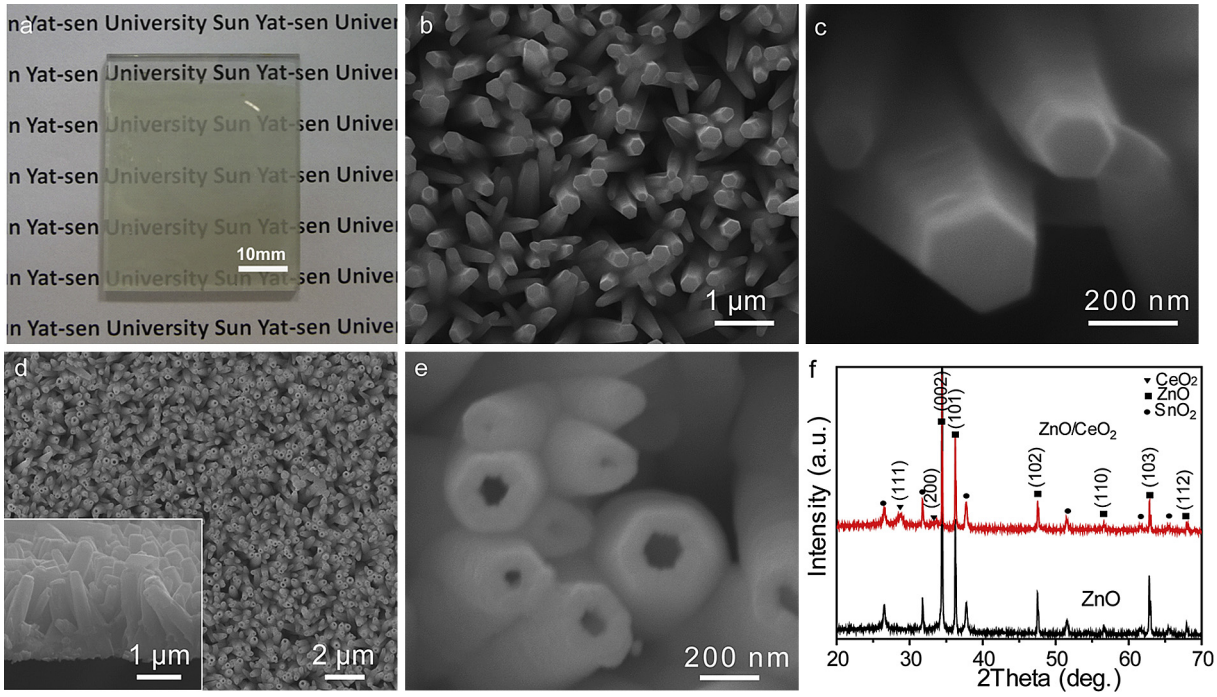

Fig. 2. (a) Photo image of CeO_2/ZnO NTA film on FTO substrate. (b, c) SEM images of ZnO NRAs. (d, e) SEM of typical CeO_2/ZnO NTAs. (f) XRD patterns of the ZnO NRAs and CeO_2/ZnO NTAs.

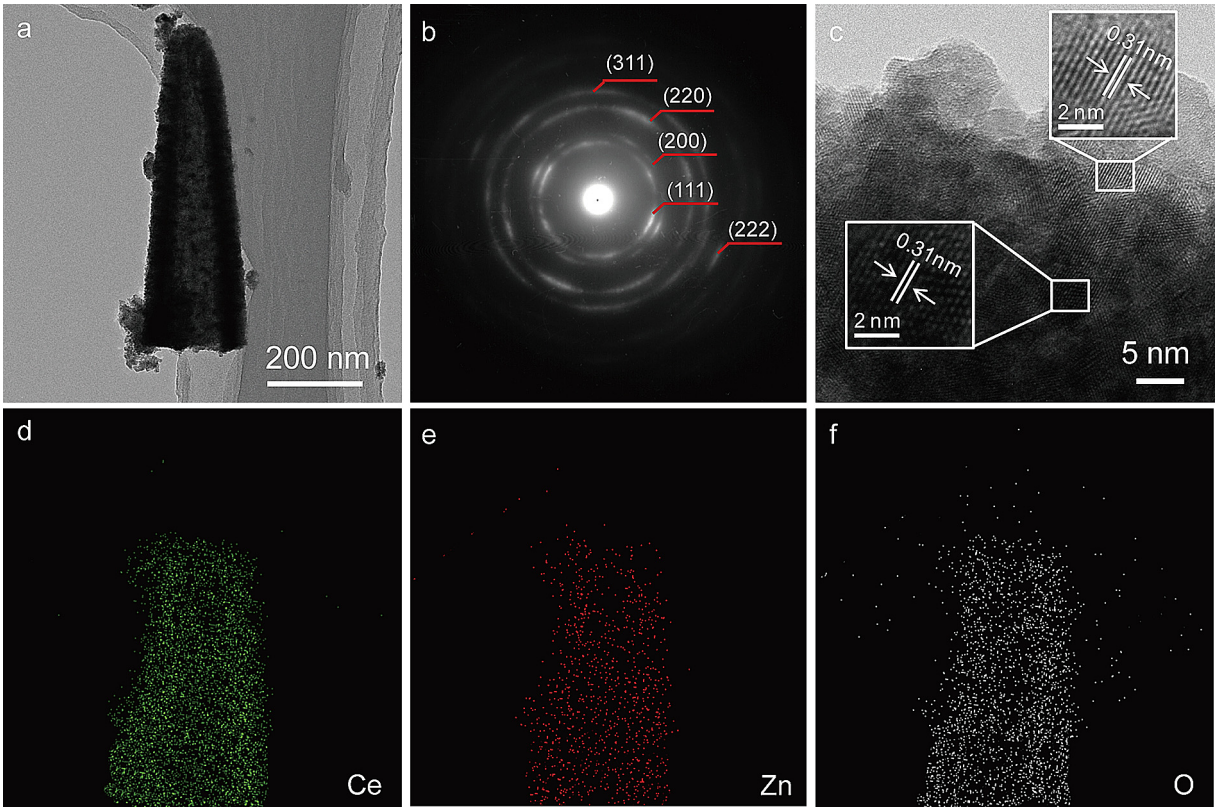

Fig. 3. (a) Conventional, (b) the corresponding SAED pattern obtained at the tip of the CeO_2/ZnO NTA film (c) lattice-resolved TEM images of CeO_2/ZnO NTA film and (d–f) EDX elemental mapping images of the Ce, Zn and O, respectively.

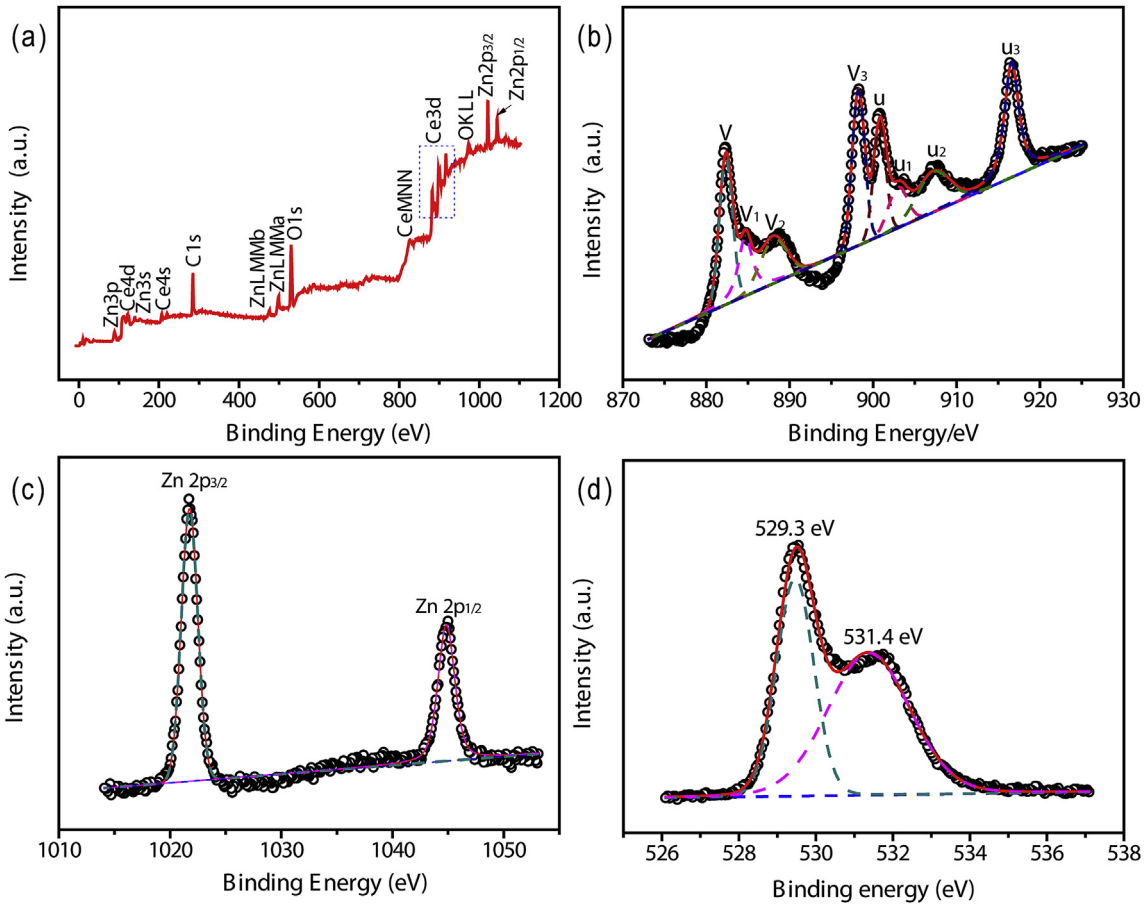

Fig. 4. (a) XPS survey, (b) Ce 3d, (c) Zn 2p and (d) O 1s core level spectra collected for the CeO_2/ZnO NTAs.

have a diameter of 150–300 nm. This clearly demonstrates that this present method can produce a good quality thin film on a large scale. Fig. 2d and e show the SEM images of CeO_2/ZnO nanotube arrays, indicating that hollow nanotubes were successfully formed after the anodic deposition. The diameter of these nanotubes was about 150–350 nm, which is similar to that of the ZnO nanorod precursors. XRD spectra collected from ZnO nanorod arrays and CeO_2/ZnO nanotubes are shown in Fig. 2f. All the diffraction peaks of ZnO nanorod arrays can be well indexed as the hexagonal wurtzite structure of ZnO (JCPDS # 36-1451). After anodic deposition in $Ce(NO_3)_3$ solution, clear diffraction peaks corresponding to cubic CeO_2 (JCPDS # 65-2975) were observed and the intensity of ZnO peaks decreased, indicating CeO_2 was formed on the ZnO. Compared with other nanotube arrays obtained via ZnO nanorod arrays as templates, the present method is a simplification because the ZnO template is directly removed during the process of anodic electrodeposition of CeO_2. The resulting large void volume provides a three-dimensional (3D) space for the mass transport of reactant and product molecules.

More detailed microstructural information of the CeO_2/ZnO nanotube films was further investigated by transmission electron microscopy (TEM). Fig. 3a shows the typical image of single CeO_2/ZnO nanotube with the diameter of ~200 nm, implying that the nanotube was successfully synthesized. A typical selected area electron diffraction (SAED) pattern of a CeO_2/ZnO nanotube was presented in Fig. 3b, which clearly demonstrates the CeO_2/ZnO nanotube is polycrystalline and CeO_2 is dominated in the prepared sample. Fig. 3c is the high-resolution TEM (HRTEM) image of a CeO_2/ZnO nanotube, disclosing that the CeO_2 layer is highly crystalline. The clear lattice fringe with a d-spacing of 0.31 nm belongs to the lattice fringe of the (111) plane of the CeO_2. Energy dispersive X-ray spectroscopy (EDX) analysis was carried out to analyze the composition of the nanotube. The elemental mapping images of this single nanotube are shown in Fig. 3d–f, clearly indicating that Zn, Ce and O are uniformly distributed throughout the entire nanotube.

In order to further study the composition of CeO_2/ZnO NTAs, X-ray photoelectron spectroscopy (XPS) was also conducted. Fig. 4a displays the XPS survey of CeO_2/ZnO NTA films. Only C, Zn and O signals are observed (C single comes from the adventitious carbon), which reveals the high purity of the sample. Fig. 4b displays the Ce 3d core level spectrum. The peaks labeled as v_1 and u_1 are the characteristic peaks of Ce^{3+} states while others are the characteristic peaks of Ce^{4+} states [21]. This indicates most of Ce ions are present in the form of Ce^{4+} states. The Zn 2p core level spectrum (Fig. 4c) shows that the Zn $2p_{3/2}$ and Zn $2p_{1/2}$ are located at binding energies of 1021.0 eV and 1044.0 eV, which are consistent with the values reported recently for ZnO [22]. The O 1s core level spectrum can be deconvolved into two peaks (Fig. 4d). The peak at 529.3 eV is a characteristic value for oxygen located in the metal oxide crystal lattice and the defect oxygen or hydroxyl groups, respectively [23]. These results clearly indicate that the prepared product is CeO_2/ZnO NTAs, which is in accordance with the TEM and EDX results.

Fig. 5 compares the UV–Vis absorption spectra of ZnO NRA and CeO_2/ZnO NTA films. The absorption band edge of CeO_2/ZnO NTA film shows a slightly red shift compared to the pure ZnO NRA film. Recent reports have shown that the transformation from Ce^{4+} to Ce^{3+} may lead to a diversification of its optical properties [24]. As

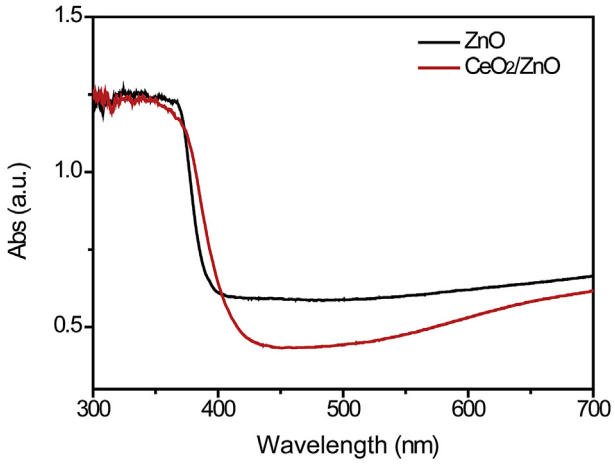

Fig. 5. UV–Vis absorption spectra of ZnO NRA film and CeO_2/ZnO NTA film.

demonstrated by XPS results (Fig. 4b), a small amount of Ce^{3+} is presented in as-prepared CeO_2/ZnO NTAs. Therefore, it may be reasonably concluded that the red-shift of the band edge results from the Ce^{4+} to Ce^{3+} transformation. This is beneficial for harvesting light during the photocatalytic process and giving high quantum efficiency for hydrogen production [6,20,25].

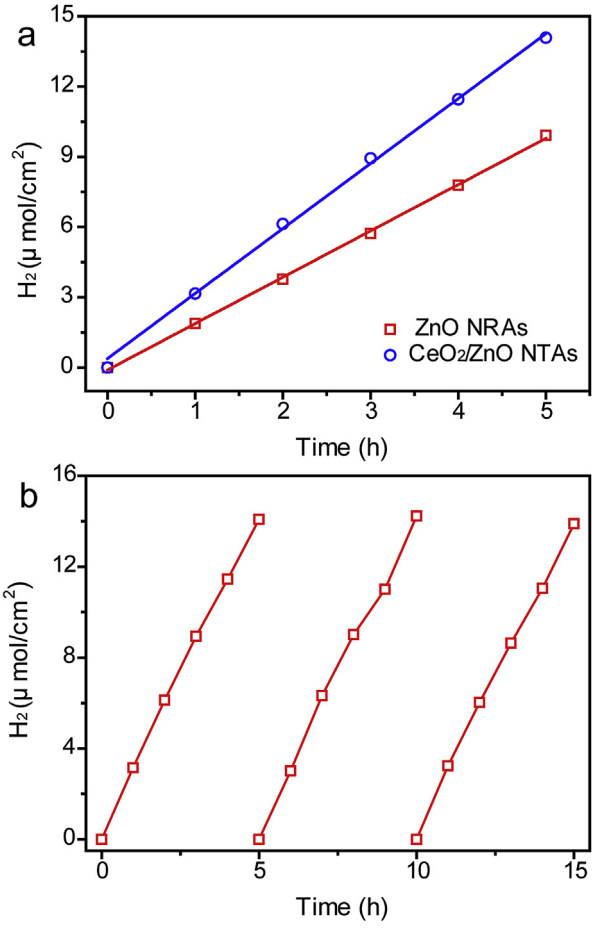

Fig. 6. (a) Photocatalytic hydrogen production rate collected for ZnO NRA film, CeO_2/ZnO NTA film in a solution containing 0.1 M Na_2S and 0.1 M Na_2SO_3 under 100 mW cm^{-2} white light irradiation. (b) Cycling performance of CeO_2/ZnO NTA film.

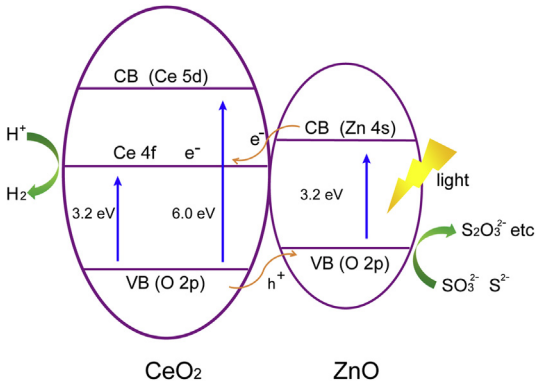

Fig. 7. Photocatalytic mechanism of hydrogen evolution on the CeO_2/ZnO NRA film.

To evaluate the photocatalytic activity of the CeO_2/ZnO NTA film, the rate of the hydrogen evolution was examined in a mixed 0.1 M Na_2S and 0.1 M Na_2SO_3 solution under 100 mW cm^{-2} white light irradiation. The time dependent rate of hydrogen evolution is showed in Fig. 6a. The ZnO NRA film has an average hydrogen evolution rate of 1.9 μmol cm^{-2} h^{-1}. Significantly, the CeO_2/ZnO NTA film achieved about 2.7 μmol cm^{-2} h^{-1}, which is nearly 40% higher than the ZnO NRA film. The efficiency of the solar to hydrogen (η) over CeO_2/ZnO nanotube array film was determined by comparing the heat of combustion of hydrogen evolved to the incoming luminous energy, and was calculated using the equation:

$$\eta = E_{H_2}/E_{solar} = [\Delta H \cdot \nu(H_2) \cdot t \cdot S]/(Ee \cdot t \cdot S) = \Delta H \cdot \nu(H_2)/Ee \quad (1)$$

where the ΔH is the standard free enthalpy change ($H_2 + 1/2O_2 \rightarrow H_2O$, −241.8 kJ mol^{-1}), $\nu(H_2)$ is average hydrogen evolution rate (2.7 μmol cm^{-2} h^{-1}) and Ee is the intensity of white light irradiation (100 mW cm^{-2}). The calculated CeO_2/ZnO nanotube array film achieves an energy conversion efficiency of 1.8%. Noteworthy is that this calculation does not consider the cathodic regeneration of the complex redox system, and the necessary anodic evolution of oxygen to complete the process. The enhanced photocatalytic activity for CeO_2/ZnO NTA film may be attributed to the following factors. First, the nanotubes have larger surface area and more active sites than nanorods. The unique nanotube structure not only allows the active species diffuse into the inside of the nanotubes, but also allows more active sites to participate in the photocatalytic reaction, hence improving the performance. Second, CeO_2 has a strong redox capability, which is an efficient catalytic material for hydrogen evolution, as recent reports have indicated [6,20]. Finally, CeO_2 can form type-II structures with ZnO, as shown in Fig. 7. Under irradiation, the photoexcited electrons produced at the conduction band of ZnO will be first transfer into the Ce 4f orbital rather than recombining with holes in the valence band of ZnO. Meanwhile, the photoexcited holes will flow from the valence band of CeO_2 to the valence band of ZnO. As a result, the formation of type-II structure can effectively suppress charge recombination, thus improving photocatalytic activity. Besides the high hydrogen evolution activity, long-term stability is another indispensable factor for a high-performance of the photocatalyst. Fig. 6b shows the rate of photocatalytic hydrogen evolution on the CeO_2/ZnO NTA film as a function of time to evaluate its stability. Hydrogen production is proportional to illumination time during the entire measurement interval, suggesting that no performance decay occurs.

Significantly, the CeO_2/ZnO NTA films developed in this work have another advantage over traditional photocatalysts, which are

usually powders, and are difficult to collect and recycle without loss, even resulting in environmental pollution. In contrast, the collection and recycling of CeO_2/ZnO NTA film in this case are very simple, since they can be removed from the cell and washed with deionized water, eliminating mass loss and environmental pollution.

4. Conclusions

In summary, we have demonstrated the design and synthesis of CeO_2/ZnO NTA films on FTO-glass substrates. These highly ordered CeO_2/ZnO NTA films with large specific area were synthesized by a two-step electrodeposition process. The photocatalytic hydrogen rate of CeO_2/ZnO NTA film reaches 2.7 μmol cm^{-2} h^{-1}, which is substantially higher than that of the corresponding ZnO NRA film. The enhancement in photocatalytic performance may be attributed to large surface areas, more reaction sites and the type-II structures which can reduce the recombination of the photoexcited electron–hole pairs. Additionally, the CeO_2/ZnO NTA films grown the FTO-glass substances show much better stability and recyclability as compared to powder photocatalysts. These findings are of great significance for the design of effective photocatalysts.

Acknowledgments

The authors acknowledge the financial support of this work by the Natural Science Foundations of China (21273290, 20973203 and 91022012), Strategic emerging industries in Guangdong Province (2011A010802004), and the Research Fund for the Doctoral Program of Higher Education of China (20120171110043).

References

[1] W.M. Singh, D. Pegram, H.F. Duan, D. Kalita, P. Simone, G.L. Emmert, X. Zhao, Angew. Chem. Int. Ed. 51 (2012) 1653–1656.
[2] G.M. Wang, Y.C. Ling, F. Qian, X.Y. Yang, X.X. Liu, Y. Li, J Power Sources 196 (2011) 5209–5214.
[3] A.I. Hochbaum, P. Yang, Chem. Rev. 110 (2009) 527–546.
[4] X. Lu, T. Zhai, H. Cui, J. Shi, S. Xie, Y. Huang, C. Liang, Y. Tong, J. Mater. Chem. 21 (2011) 5569–5572.
[5] J.H. Park, S. Kim, A.J. Bard, Nano Lett. 6 (2005) 24–28.
[6] N. Chouhan, C.L. Yeh, S.-F. Hu, R.-S. Liu, W.-S. Chang, K.-H. Chen, Chem. Commun. 47 (2011) 3493–3495.
[7] N.K. Shrestha, K. Lee, R. Hahn, P. Schmuki, Electrochem. Commun. 34 (2013) 9–13.
[8] X. Qi, G. She, M. Wang, L. Mu, W. Shi, Chem. Commun. 49 (2013) 5742–5744.
[9] H. Dang, X. Dong, Y. Dong, J. Huang, Int. J. Hydrogen Energy 38 (2013) 9178–9185.
[10] J. Goldberger, R. He, Y. Zhang, S. Lee, H. Yan, H.-J. Choi, P. Yang, Nature 422 (2003) 599–602.
[11] J.H. Lim, J. Choi, Small 3 (2007) 1504–1507.
[12] J. Su, L. Guo, N. Bao, C.A. Grimes, Nano Lett. 11 (2011) 1928–1933.
[13] S.U.M. Khan, M. Al-Shahry, W.B. Ingler, Science 297 (2002) 2243–2245.
[14] H.M. Chen, C.K. Chen, Y.-C. Chang, C.-W. Tsai, R.-S. Liu, S.-F. Hu, W.-S. Chang, K.-H. Chen, Angew. Chem. Int. Ed. 122 (2010) 6102–6105.
[15] J.A. Seabold, K.-S. Choi, J. Am. Chem. Soc. 134 (2012) 2186–2192.
[16] Y.C. Qiu, W. Chen, S.H. Yang, J. Mater. Chem. 20 (2010) 1001–1006.
[17] Y.C. Qiu, K.Y. Yan, H. Deng, S.H. Yang, Nano Lett. 12 (2012) 407–413.
[18] C. Ho, J.C. Yu, T. Kwong, A.C. Mak, S. Lai, Chem. Mater. 17 (2005) 4514–4522.
[19] A. Primo, T. Marino, A. Corma, R. Molinari, H. García, J. Am. Chem. Soc. 133 (2011) 6930–6933.
[20] X.-H. Lu, S.-L. Xie, T. Zhai, Y.-F. Zhao, P. Zhang, Y.-L. Zhang, Y.-X. Tong, RSC Adv. 1 (2011) 1207–1210.
[21] P. Burroughs, A. Hamnett, A.F. Orchard, G. Thornton, J. Chem. Soc. Dalton Trans. (1976) 1686–1698.
[22] X. Lu, G. Wang, S. Xie, J. Shi, W. Li, Y. Tong, Y. Li, Chem. Commun. 48 (2012) 7717–7719.
[23] H.-I. Chen, H.-Y. Chang, Solid State Commun. 133 (2005) 593–598.
[24] P. Patsalas, S. Logothetidis, C. Metaxa, Appl. Phys. Lett. 81 (2002) 466–468.
[25] M.Y. Chen, X.T. Zu, X. Xiang, H.L. Zhang, Phys. B Condens. Matter 389 (2007) 263–268.